2024 IEEE/ASME International Conference on Advanced Intelligent Mechatronics (AIM)
July 15-19, 2024. Boston, MA, USA

Task Sensing and Adaptive Control for Mobile Manipulator in Indoor Painting Application

Yadan Zeng[1], Dingyuan Zhang[1], Shao-Yu Chien[2], Hendra Suratno Tju[1], Carlo Wiesse[3], Feng Cao[3], Jiadong Zhou[1], Xiaohan Li[4], I-Ming Chen[1], *Senior Member, IEEE*

***Abstract*— Robotic painting, particularly in industrial and construction domains, has attracted considerable attention due to its precision and uniformity. However, current systems are constrained by inadequate precision and effectiveness in painting, particularly when applied to large-scale surfaces. This study introduces an advanced adaptive robotic painting system that incorporates a mobile manipulator (MM) designed to enhance both accuracy and efficiency in indoor surface painting through two innovative sub-modules: automated trajectory generation and MM adaptive control policy (ACP). Initially, to autonomously generate the accurate trajectory, we propose the Attention-aware Graph Network (AGN) for refining 3D surface model to significantly enhance the accuracy and efficiency of environment modeling. Following this, the RayCast 3D Mapping technique is introduced for precise projection of 2D images onto arbitrary 3D surfaces with its flexibility and adaptability. Furthermore, we introduce an MM ACP comprising a trajectory controller and a close-loop whole-body controller. This dual-controller system enables the MM to swiftly move to target poses and smoothly follow trajectories, with the capability to autonomously switch between control paradigms based on task requirements. In addition, Experimental results demonstrate that the proposed automated trajectory generation strategy, coupled with the MM ACP, significantly improves the accuracy of environmental perception and the efficiency of trajectory generation. Furthermore, the MM exhibits robust performance in both simulated and real-world settings, successfully executing fully autonomous painting tasks.**

I. INTRODUCTION

Mobile manipulators (MMs), integrating the dexterity of robotic arms with the flexbility of mobile platforms, exhibit a versatility compared to stationary robots. The additional degrees of freedom (DOFs) provided by the mobile platform enable these high-redundancy manipulators to perform a wider variety of tasks, offering numerous solutions in their application areas [1], [2]. Contrary to applications centered around pick-and-place tasks [3], which focus primarily on

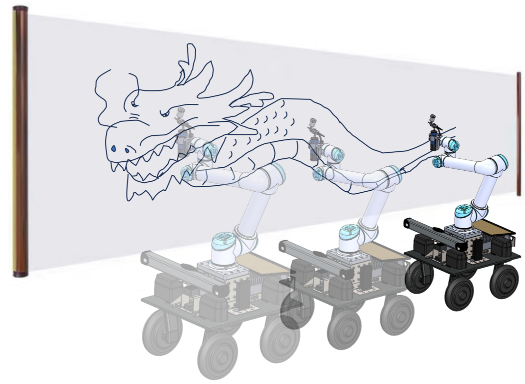

Fig. 1. Robotic painting system is applied on the large-scale wall painting tasks with the predefined pattern.

tasks such as painting, welding, and drawing [4], [5], require the MM to have the additional capability to generate continuous operating trajectories that align with the environment or target objects, as well as the precise tracking of these paths. Consequently, the ability of MMs to seamlessly switch between operational modes is essential for tasks like large-scale wall painting, as illustrated in Fig.1.

The field of robotic painting has attracted considerable attention in the industrial and construction field due to its exceptional precision and uniformity. Regarding large-scale painting applications, painting robots can be classified into three principal categories: Track-Mounted Robots [6], [7], Multi-Arm Robots [8], and Mobile Manipulators [1], [4], [9]. The first two categories represent traditional painting robot solutions, primarily expanding operational reach through the construction of tracks or leveraging multiple robotic arms for extended range. However, such methods are limited by space requirements and coordination complexity. In recent years, the adoption of MMs for painting tasks has increasingly popular, combining the mobility of autonomous robots with the accuracy of articulating arms. Nevertheless, current MMs follow a “park-operate-park” mode, executing segmented, phased trajectory planning based on surface slicing technology to accomplish extensive range painting, facing accuracy challenges at segmented task transitions. [4]. Consequently, the primary challenge for current MMs lies in enhancing the precision of both trajectory generation and overall trajectory tracking. To address this, we propose an MM designed to operate while in motion, outfitted with two sub-modules: automated trajectory generation and MM adaptive control policy (ACP), aimed at augmenting the accuracy of indoor surface painting.

Firstly, the automated generation of painting trajectories

*This project is supported by A*STAR under “RIE2025 IAF-PP Advanced ROS2-native Platform Technologies for Cross sectorial Robotics Adoption (M21K1a0104)” programme, Corresponding authors: Yadan Zeng Email:yadan001@e.ntu.edu.sg

[1] Y. Zeng, D. Zhang, H. Tju J. Zhou and I-M. Chen are with the Robotics Research Centre of the School of Mechanical and Aerospace Engineering, Nanyang Technological University, Singapore. Corresponding authors: Yadan Zeng and Houde Dai.

[2]S. Chien is with the Department of Electrical and Computer Engineering, Tamkang University, New Taipei City, Taiwan.

[3]C. Wiesse and F. Cao are with the Institute of Advanced Remanufacturing and Technolody Center (ARTC), Agency for Science, Technology and Research (A*STAR), 3 Cleantech Loop, 01/01 CleanTech Two, Singapore 637143.

[4]X. Li is with the College of Information and Control Engineering, Xi’an University of Architecture and Technology, Xi’an, China.

relies on the integration of precise 3D surface modeling and advanced image mapping techniques. Traditionally, 3D models creation for large-scale painting has relied on manual, standalone 3D scanners, requiring further calibration for robot manipulation, thereby complicating the overall process [9], [10]. To acquire real-time surface data, an advanced technique involves the integration of RGB-D cameras with MMs. However, the precision of 3D surface data captured by these compact cameras [11], is often suboptimal, significantly impacting the accuracy of trajectories generated for subsequent operations. Thus, the refinement of this data is crucial for improving the accuracy of surface model. Traditional refinement methods, such as super-voxel structures, require a significant time and are not suitable for real-time applications [12], [13]. In contrast, deep-learning-based methods especially end-to-end networks provide enhanced effectiveness but may not completely resolve irregularities in point clouds, which can affect the quality of refinement [14], [15]. Addressing this limitation, we propose the development of an Attention-aware Graph Network (AGN) designed for selective feature extraction and refinement in point clouds, focusing on noise correction, thereby substantially enhancing the accuracy of 3D surface reconstructions for large-scale painting applications. Alongside 3D modeling challenges, the precise projection of 2D images onto 3D surfaces for indoor robotic painting requires meticulous mapping techniques [16]. Traditional approaches such as least squares conformal mapping, aiming to preserve geometric accuracy through mesh reconstruction, often lead to inconsistencies in mapping because of the surface parameterization and subsequent mapping procedure [17]. In contrast, the process of mapping the 3D surface onto a 2D plane, overlaying the 2D picture onto it, and subsequently remapping it back to 3D to produce the trajectory of the painting involves the handling of additional 3D data and poses difficulties when dealing with surfaces that have irregular shapes [5]. To mitigate these issues, we introduce the RayCast 3D Mapping method, which employs ray casting principles [18] to optimize the mapping procedure by focusedly interacting with point cloud data relevant to predetermined patterns. This technique not only streamlines data processing but also accommodates various image resolutions and complex surface geometries, enhancing its applicability across diverse robotic painting scenarios.

Secondly, the effectiveness of MMs in large-scale automated painting depends on their ability to execute paths with precision. In the conventional manner, MMs operate with segregated control systems for the mobile base and the manipulator arm [19], leading to challenges, including the occurrence of discontinuities or overlaps in painted areas. Specifically, whole-body control MMs typically concentrate on pick-and-place tasks, facilitating path planning and ensuring the maintenance of movement speed [20]–[22]. However, at low-speed trajectory tracking, the base odometry's sensitivity to minor movements is insufficient, potentially leading to inaccuracies in odometry and, by extension, overall trajectory tracking. Addressing this challenge necessitates the MM's ability to adaptively switch between different control modes based on the task, with a particular emphasis on compensating odometry in whole-body control during trajectory tracking. To this end, we propose an adaptive control strategy that enable smoothly switching between control modes and incorporating close-loop control for enhanced odometry compensation. This approach significantly improves the MM's ability to reach target poses and follow trajectories with high precision.

Finally, we have designed a MM comprising a robot manipulator and a four-wheel drive mobile robot, equipped with target sensing, trajectory generation, and adaptive control mechanisms to achieve the autonomous indoor painting. Moreover, comprehensive experimentation with a custom MM highlights the precision and autonomy of our system in executing painting tasks. The evaluation framework incorporates simulations to evaluate the adaptability of the system over various wall types, as well as empirical testing in real-life settings using the custom MM. This work contributes in three significant ways:

- We propose an Attention-aware Graph Network (AGN) for 3D surface modeling to refine the captured 3D surface, ensuring the accuracy of the painting trajectory. The RayCast 3D Mapping technique is proposed to improve the efficiency of trajectory generation, addressing the challenges of irregular surfaces and enhancing overall system performance in complex environments.
- We developed an adaptive control policy that integrates a trajectory controller and a closed-loop whole-body controller to maintain precise operations during low-speed following tasks. This dual-controller setup allows the robot to quickly achieve target poses and ensures accurate, smooth trajectory tracking.
- We evaluate our MM on indoor painting tasks across both simulated and physical environments. The results indicate that the MM effectively produces dynamic end-effector painting trajectories and demonstrates high accuracy and smoothness in trajectory tracking. This comprehensive assessment validates the efficiency of the technology and highlights its potential for realistic painting applications or comparable real-world scenarios.

II. System Overview

As depicted in Fig. 2, we present a comprehensive overview of our robotic painting system, detailing the process of rendering a painting on an arbitrary surface, utilizing a customized MM that encompasses both a robotic manipulator and a mobile platform. This system is particularly optimized for large-scale indoor painting applications, necessitating the accurate modeling of the painting surface, the generation of a 3D painting trajectory, and the smooth execution of the painting task.

Given that the indoor painting area typically exceeds the robot's range, our approach involves deploying the robot across multiple waypoints to conduct comprehensive area

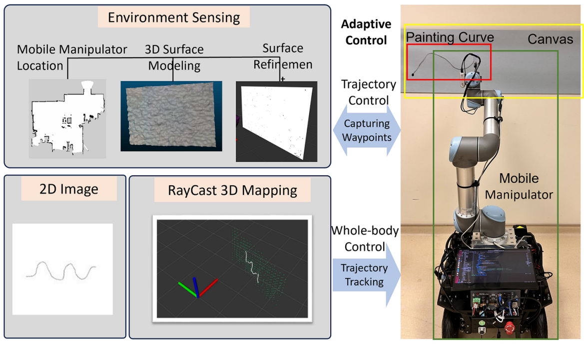

Fig. 2. Flowchart of task sensing and adaptive control for mobile manipulation in indoor painting application.

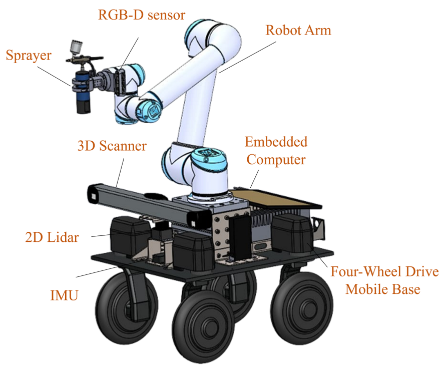

Fig. 3. Mobile manipulator and the components.

scanning and localization through an onboard RGB-D camera. These strategically determined waypoints, represented as $C \subset \mathbb{R}^6$, are optimized to minimize the number of captures required while ensuring complete coverage of the operating area. The trajectory controller is activated via ACP to guide the robot to achieve the target waypoints C. At each waypoint C_i, the system acquires target surface data $S_i \subset \mathbb{R}^{3\times n}$ in point cloud format and aligns them to S. However, due to the inherent limitations of RGB-D sensors, the initial quality of S may not meet the exacting standards required for painting. Therefore, a refinement process transforms S to S' to meet the requirements of the painting task.

Following this preparatory phase, a 3D painting trajectory is formulated for the designated images, represented as $\mathscr{P} \subset \mathbb{R}^2$. To map this 2D image onto a 3D surface of arbitrary orientation and size, we introduce the RayCast 3D Mapping methodology. This method projects the $\mathscr{P}$ onto the 3D surface, thereby deriving the painting trajectory $T \subset \mathbb{R}^6$. The orientations of each T_i are estimated according to the normal vector for each point in S', which is essential for determining the orientation of the end-effector. Upon computing the 3D trajectory for painting, it autonomously switches to whole-body control through ACP to follow this trajectory. The collaborative interaction between 3D painting trajectory generation—incorporating both 3D surface modeling and RayCast mapping—and the adaptive control policy, alternating between trajectory and whole-body controllers, guarantees the accuracy and efficiency of automated indoor painting. The structure of custom MM is illustrated in Fig. 3.

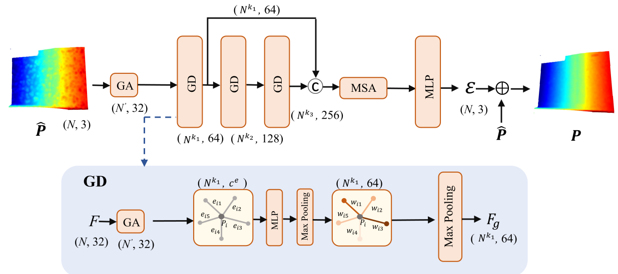

Fig. 4. Struction of the Attention-aware Graph Network.

III. 3D Painting Trajectory Generation

3D Painting Trajectory Generation is essential in the execution of indoor painting tasks. It contains both the processes of 3D surface modeling and the mapping from 2D images to 3D surfaces. Instead of using separate systems for surface capture, our technique incorporates this functionality directly into the robotic system. This integration significantly enhances operational efficiency and flexibility while simultaneously mitigating errors associated with the calibration between distinct systems. Furthermore, the ray casting technique is adopted to align the 2D image on the 3D surface to generate the operating trajectory, guaranteeing accurate alignment and orientation, which is crucial for carrying out the painting process.

A. 3D Surface Refinement

The point cloud obtained from the RGB-D camera consistently fails to meet the criteria for painting. The technique of refining 3D surfaces model S to refined surface S' is crucial for motion planning in robotic painting. The utilization of Graph Neural Networks (GNNs) presents a highly efficient method of processing irregular and unordered structures, such as point clouds. Moreover, the incorporation of attention-aware neural networks in point cloud refinement enables models to choose focus computational resources on different regions of the input data. Through the utilization of the attention mechanism, the model effectively evaluates the importance of different points, guiding attention towards regions that need to be corrected.

In this study, we introduce an innovative framework, the Attention-aware Graph Network (AGN) as depicted in Fig. 4, specifically designed for the extraction of 3D shape features from point clouds. The AGN methodology emphasizes a dual-focus approach, incorporating both self-attention mechanisms and adjacent information. This is accomplished by utilizing a graph attention mechanism, which allows each local feature vector to explore various locations, thereby facilitating the identification and integration of connections between local and global features.

Our method focuses on strategically utilizing the inherent geometric features seen in point clouds. To accomplish this, we have developed the Hierarchical Feature Extractor (HFE) which includes 3 Graph Descriptors (GDs). The GD leverages an attention-based methodology to effectively aggregate local graphs, thus enhancing the feature extraction process. The AGN processes the graph representation of the input

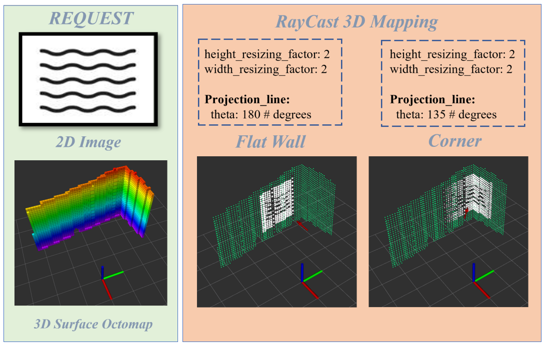

Fig. 5. Illustration of rayCast 3D mapping technique for projecting a 2D image onto varied surface geometries.

point cloud, enabling the extraction of both global and local point cloud features. Integrating an attention mechanism, the AGN effectively identifies and emphasizes key noise area within the point cloud. The network approximates the physical residuals in the input point cloud, which may arise from the principles of RGB-D depth image acquisition, inherent structural errors in the camera, or random errors encountered during the data collection process. These residuals are then compensated in the original point cloud, resulting in a refined point cloud with enhanced accuracy, thereby achieving the objective of refining the target surface.

During the training phase of our model, we utilized two metrics to ensure the precision and quality of the generated point clouds: the Chamfer Distance with $L2$ norm and the Laplacian Smoothness Loss. The Chamfer Distance with $L2$ norm can be defined as:

$$\mathscr{L}_{CD_2}(\mathbf{P},\mathbf{Q}) = \frac{1}{|\mathbf{P}|}\sum_{x\in\mathbf{P}}\min_{y\in\mathbf{Q}}\|x-y\|_2^2 + \frac{1}{|\mathbf{Q}|}\sum_{x\in\mathbf{Q}}\min_{y\in\mathbf{P}}\|y-x\|_2^2, \quad (1)$$

where $\|\|_2^2$ represents the squared $L2$ norm, accentuating the Euclidean distance between point pairs. The Laplacian Smoothness Loss is adopted to evaluate and improve the smoothness of the point cloud, which is given by:

$$\mathscr{L}_{smooth} = \sum_{i=1}^{N}\left\| p_i - \frac{1}{K}\sum_{k=1}^{K} p_{i_k} \right\|^2. \quad (2)$$

Consequently, the aggregated loss function is expressed as:

$$\mathscr{L} = \mathscr{L}_{CD_2}(\mathbf{P},\mathbf{Q}) + \mathscr{L}_{smooth}. \quad (3)$$

B. RayCast 3D Mapping

We propose a more direct and flexible approach: the RayCast 3D Mapping method, grounded in the principles of ray casting. This method as shown in Fig. 5 initializes ray origins aligned with the normal of the image plane. It then calculates the mapping of the 2D image $\mathscr{P}$ onto the surface S' by aligning these rays with the normal vector of each point on the S'. The projected points T are systematically arranged to form a trajectory that encompasses all points, optimized through a sorting algorithm to minimize the overall trajectory length.

For the execution of these points, we employ a distance sorting algorithm to further reduce the trajectory length. The 2D image is segmented according to conventional drawing and writing patterns, extracting a series of segments. These segments are then sequentially integrated into the path generation process, thereby endowing the robotic painting operation with a human-like execution quality. A critical component of the RayCast 3D Mapping algorithm is the ray casting process itself, defined as:

$$\mathbf{T_i} = Ray\mathbf{O} + \mathbf{t}\cdot\mathbf{RayV}, \quad (4)$$

where t represents the parameter that allows for the intersection of the ray with the plane. Each individual ray vector is methodically analyzed in order to identify the nearest point inside the point cloud. This involves the calculation of the interaction point between each ray and the point cloud. A crucial element of our methodology involves the systematic assessment of locations where two or more components intersect. The prioritization method places emphasis on points that are in close proximity to the origin of the ray, while discarding locations based on specific criteria such as pixel intensity and spatial positioning in reference to the map frame.

IV. MM Adaptive Control Policy

For autonomous indoor operations with MMs, there typically exist two primary motion modes: pose achievement and trajectory following [23], [24]. Pose achievement, focusing on precise location and orientation, typically employs separate controls for the mobile base and the robot arm, facilitating efficient navigation and precise positioning in constrained environments. Trajectory following, however, requires a comprehensive control system for smooth, coordinated movements essential for dynamic activities like real-time tracking or manipulation. Within indoor painting applications, these modes are crucial for complex operations including autonomous target modeling, trajectory generation, and subsequent trajectory tracking. To seamlessly integrate these capabilities, an ACP combined with a trajectory controller and a closed-loop whole-body controller has been developed, enabling MMs to autonomously switch between motion modes based on specific painting task demands, thereby significantly enhancing operational adaptability and intelligence for fully automated tasks.

For a given series of operational waypoints, represented as a sequence of poses (position and orientation), we employed K-means clustering to uncover underlying patterns. Given a set of N poses, K-means aims to partition the data into K clusters by minimizing the within-cluster variance. The objective function of K-means clustering is formulated as follows:

$$\arg\min_{C}\sum_{k=1}^{K}\sum_{i=1}^{N}\|x_i-\mu_k\|^2, \quad (5)$$

where C denotes the cluster assignment matrix, $C_{ik}=1$ if pose i belongs to cluster $\mathscr{K}$, and μ_k represents the centroid of $\mathscr{K}$. The algorithm iteratively optimizes cluster assignments and updates centroids until convergence.

Subsequently, Principal Component Analysis (PCA) was conducted on each cluster to quantify variance differences. The variance ratio difference for each cluster calculated to

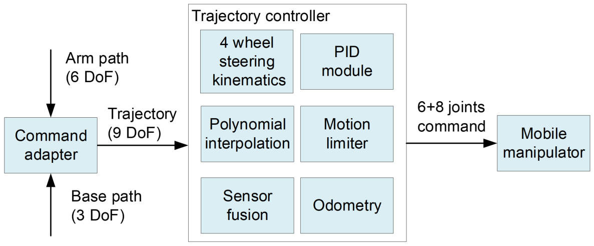

Fig. 6. Schematic of the trajectory control architecture for the mobile manipulator.

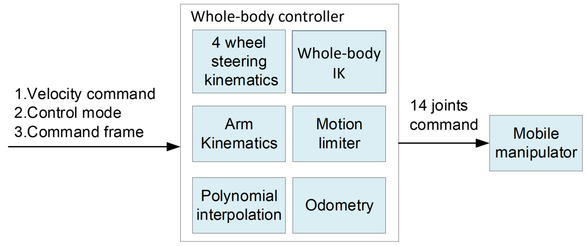

Fig. 7. Schematic of the whole-body control architecture for the mobile manipulator.

measure dispersion across the principal components was computed as:

$$V_{diff_i} = \mathbf{std}(PC_{1_i}, PC_{2_i} ..., PC_{n_i}), \tag{6}$$

where PC_{n_i} represents the variance ratio of the n^{th} principal component of the i^{th} cluster, and i ranges from 1 to K. The average variance difference across all clusters was determined by:

$$V_{diffavg} = \frac{1}{k}\sum_{i=1}^{K} V_{diff_i}, \tag{7}$$

highlighting the uniformity of distribution within clusters. For independent poses, their variance differences remained within a specific range, while poses belonging to a path exhibited either very small or significantly large variance differences. These differences indicate paths with minimal directional change or those with substantial rotational movements, respectively. Based on empirical observations, we set upper bounds (0.8) and lower bounds (0.3) for mode differentiation.

A. Trajectory Controller

In the proposed trajectory controller for a mobile manipulator, the system decomposes a designated path into discrete commands for both the mobile base and the robot arm. This decouples the 9-DOF path into separate 6-DOF for the arm and 3-DOF for the base, with subsequent trajectory calculations performed by modules like MoveIt for the arm and Nav2 for the base. These are harmoniously integrated by the command adapter, which ensures seamless motion coordination (Fig. 6).

The command adapter focuses on unifying these disparate trajectories generated by MoveIt and Nav2 into a unified trajectory by standardizing time parameters and ensuring kinematic consistency across state vectors ($\mathbf{s}(t) = [\mathbf{p}(t), \mathbf{v}(t), \mathbf{a}(t)]$ where $\mathbf{p}(t)$, $\mathbf{v}(t)$, and $\mathbf{a}(t)$ represent position, velocity, and acceleration vectors, respectively). By harmonizing the time frames of each trajectory, it achieves time coherence, which is a vital requirement for the smooth integration of motion trajectories. The core of the method lies in the interpolation of state vectors at standardized intervals, ensuring that the produced trajectory satisfies with both kinematic continuity and dynamic constraints.

For our mobile base employing a Four-Wheel Drive mechanism, the Four-Wheel Steering Kinematics (4WSK) is essential. The 4WSK allows for independent steering of each wheel, which provides greater flexibility and agility in navigation. It intricately converts the 3-DOF trajectory into precise 8-DOF commands, deriving the rotational angle of each wheel θ_i and the steering angle φ_i relative to the x-axis of the robot's frame, ensuring precise motion control. Similar to [25], define the velocity of the mobile base as:

$$v_r = \begin{bmatrix} v_{rx} & v_{ry} & \omega_r \end{bmatrix}^T, \tag{8}$$

where v_{rx} and v_{ry} represent the translational velocity in the x_r and y_r directions, respectively. ω_r represents the angular velocity of the body platform relative to vertical z_r-axis. The relationship between the angular velocity of individual wheels $(\dot{\theta}_i, \dot{\varphi}_i)$ and the total velocity of the mobile base can be established as:

$$\begin{bmatrix} \dot{\theta}_i \\ \dot{\varphi}_i \end{bmatrix} = \frac{1}{rl} \begin{bmatrix} lC\varphi_i & -lS\varphi_i & a_i lS\varphi_i - b_i lC\varphi_i \\ rS\varphi_i & rC\varphi_i & lr + brS\varphi_i - arC\varphi_i \end{bmatrix} \begin{bmatrix} v_{rx} \\ v_{ry} \\ \omega_r \end{bmatrix}, \tag{9}$$

where S and C symbolize sinusoidal and cosinusoidal functions, respectively. r and l the wheel radius and steering link length, respectively. (a_i, b_i) indicate the coordinates relative to the body frame of the mobile base, where i ranges from 1 to 4. Thus upon function (9), the angular and steering angles can be computed, so enabling their transformation into instructions for controlling the speeds of 8 joints.

B. Closed-loop Whole-body Controller

When it comes to MM operations, it is essential to use a whole-body control scheme to ensure the accurate positioning of the end-effector. Our technique is centered around the integration of Whole-Body Inverse Kinematics (WBIK) and 4WSK, forming the foundation of our 14-joint command strategy as depicted in Fig. 7. Our WBIK methodology, which draws inspiration from the quadratic programming (QP) framework proposed by [26], adeptly addresses the inherent challenges of WBIK inherent to MMs with a combined 9 DoF. The QP technique is established as an optimization problem, calculating joint velocities with precision to realize the desired end-effector velocity while conforming to constraints that prevent joint limit violations and enhance manipulability. However, this QP-WBIK strategy encounters challenges during low-speed tasks, such as painting, where the combination with 4WSK can result in discontinuous base motion. To address this, we incorporate dynamical constraints for the base's movement, optimizing the base's actions in minimal motion scenarios by calibrating the movement amplitude during trajectory tracking. The optimization problem, therefore, involves these dynamics and

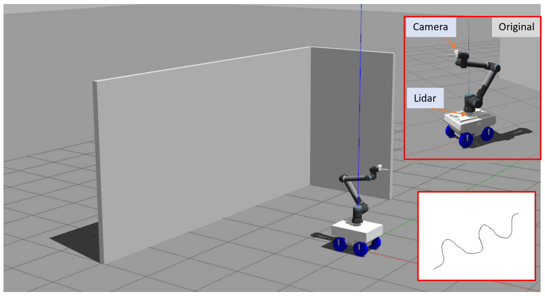

Fig. 8. Simulation screenshot in gazebo of the indoor painting setup. The robot is equipped with a hand-mounted camera and LIDAR for navigation and the 2D painting pattern is pre-provided.

c

is concisely formulated as:

$$\min_{\mathbf{q}} \frac{1}{2}\mathbf{q}^{\mathbf{T}}\mathscr{M}\mathbf{q}+\mathbf{C}^{\mathbf{T}}\mathbf{q} \tag{10}$$

subject to

$$\mathbf{Jq}={}^{\mathbf{b}}\mathbf{v}_{\mathbf{e}}, \quad \mathbf{Aq}\leq\mathbf{B}, \quad \mathbf{Q}'_{\min}\leq\mathbf{q}\leq\mathbf{Q}'_{\max} \tag{11}$$

where $\mathbf{q}$ is the vector of joint velocities for both the arm and the base, $\mathbf{Q}$ is a positive semidefinite matrix defining the cost associated with the velocities, $\mathbf{C}$ represents additional costs such as manipulability. $\mathbf{A}$ and $\mathbf{B}$ define the inequality constraints such as joint limits, and $\mathbf{Q}'_{\min}$, $\mathbf{Q}'_{\max}$ are the bounds on the joint velocities, where the lower bounds are updated based on the desired movements in the x and y directions, which are defined as:

$$\mathbf{Q}'_{\min}[0,1]=[\mathscr{S}(\Delta x),\mathscr{S}(\Delta y)], \tag{12}$$

where $\mathscr{S}(\cdot)$ is the scaled oprator. Δx and Δy are the differences in the x-coordinate and y-coordinate of the end-effector position, respectively. In addition, the control logic for low-speed MM movement incorporates a threshold-based halting mechanism, expressed as:

$$\text{if } \Delta x_{\text{total}}\geq\Theta \text{ then} \begin{cases}\text{halt base,}\\ \Delta x_{\text{total}}\leftarrow 0\end{cases}. \tag{13}$$

In this design, $\Delta x_{total}=\sqrt{\Delta x^2+\Delta y^2}$ aggregates the displacement of mobile base, triggering a halt in base movement upon reaching the predefined threshold Θ. This mechanism's activation depends on the complexity of the target trajectory, privileging the manipulator's involvement in following trajectory exhibiting significant local variance and thus in turn reduces the frequency of base activations. By implementing this closed-loop control technique, the MM system consistently maintains precise operations, especially when performing tasks that require low-speed following. This enhances the overall accuracy and effectiveness of the system in following to the desired trajectory.

V. Experiment And Results

To validate the tracking performance of the devised task sensing and ACP for an autonomous MM in an indoor painting application, a comprehensive suite of experimental verifications has been conducted. These experiments were performed using our custom-designed MM. Both simulation and real-world trials demonstrated the effectiveness of the fully automated indoor painting procedure. Furthermore, the efficacy of the 3D surface refinement and RayCast 3D Mapping techniques has been well illustrated.

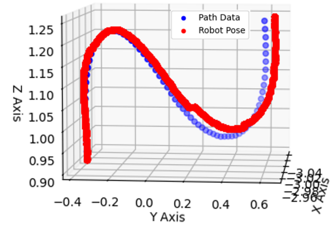

Fig. 9. Closed-loop Whole-Body Controller-Based Trajectory Tracking Experiment in Gazebo. The red curve is the generated path and the blue one is the executed path in 3D space.

TABLE I

RMSE of Trajectory Tracking Error in Simulation

Error(m)	X	Y	Z	Total
RMSE	0.021	0.025	0.026	0.024

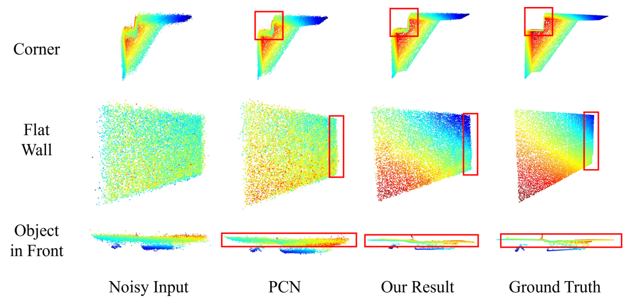

Fig. 10. Results of point cloud refinement base on AGN and PCN. The scenerios including the corner, the flat wall, and the object infront of a flat wall are illustrated.

A. Simulation

Fig. 8 presents a screenshot of a simplified indoor painting scene within the Gazebo simulation environment. The scene is configured with two walls forming a planar surface and a corner. A MM is positioned nearby to execute the painting task. This task adheres to the framework depicted in Fig. 2.

Fig. 9 and Table I illustrate the results of the robot's trajectory tracking. During this process, the robot employs a closed-loop whole-body controller and interpolates the predefined trajectory to ensure smoother motion. The Root Mean Square Error (RMSE) values for the X, Y, and Z axes are computed to assess the tracking accuracy. It is observed that the robot proficiently follows the preset trajectory, with an overall error margin of 0.024 meters.

B. Point cloud Refinement

The Attentional Graph Network (AGN) is employed to refine input low-precision point clouds. The AGN-based point cloud refinement capability was evaluated in indoor scenarios. Implementation was carried out on a standard workstation configured as follows:

- Memory: 64 GB

TABLE II
CHAMFER DISTANCE(CD) (1E-3) RESULTS OF SURFACE REFINEMENT THROUGH AGN

Method	L_1 norm	L_2 norm
Noisy input	25.88	5.08
Refinement result	5.52 (78.7%)	1.12 (77.9%)

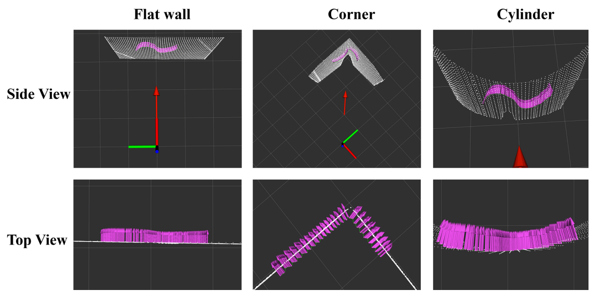

Fig. 11. Trajectories Generated in Varied Scenarios: Flat Wall, Corner, and Cylinder. This figure presents both the side and top views of the trajectories, illustrating the orientation of each point within the path.

- Processor: Intel® CoreTM i9-9900K CPU @ 3.6GHZ
- GPU: Quadro RTX 4000
- Operating System: Ubuntu 18.04

Three distinct scene types were captured using an on-hand Realsense RGB-D camera: a flat wall, a corner, and objects placed in front of a wall. Ground-truth point clouds were captured using a Photoner 3D scanner mounted on the robot. The transformation between these two frames was provided in real-time by the robot system. The results of the AGN-based point cloud refinement and the comparison with PCN are presented in Fig. 10. It is evident that the proposed method significantly enhances point cloud quality, particularly in areas with distinct geometric features such as edges and corners. Table II lists the differences and the improvement percentages between the original point clouds captured by the RGB-D camera and the refined point clouds compared to the ground truth. We used the Chamfer Distance with L_1 and L_2 norms as criteria, achieving improvements of 78.7% and 77.9%, respectively. This indicates that the accuracy of 3D surface models is greatly increased by the AGN-based point cloud refinement method, thereby enhancing the accuracy of the generated trajectory.

C. Raycast 3D mapping

In this study, we evaluated the efficacy of the Raycast 3D mapping method within a simulated environment. The simulation involved setting up a canvas on various structures: a flat wall, a corner, and a cylinder, using a basic painting pattern: a curve.

Fig. 11 illustrates the trajectories generated in these three distinct scenarios. The paths were devised based on the specific location and size of each canvas. Our methodology incorporated the use of a cosine metric to ascertain the closest point in the point cloud to our projection line. A critical aspect of this process involved calculating the normal at each point to ensure perpendicularity to the wall surface. This is a pivotal consideration for tasks such as painting or drawing, where it is imperative to maintain the end effector's perpendicular orientation to the surface for precision and to prevent damage during contact tasks. These results highlight how Raycast 3D mapping can improve the accuracy and adaptability of robotic operations in complex spatial configurations.

TABLE III
RMSE OF TRAJECTORY TRACKING ERROR IN REAL ROBOT

Error(m)	X	Y	Z	Total
RMSE	0.010	0.040	0.019	0.046

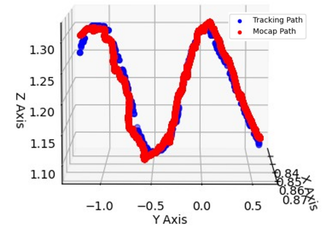

Fig. 12. Closed-loop Whole-Body Controller-Based Trajectory Tracking Experiment in Real Scene. The red curve is predefined path and the blue one is the executed path in 3D space.

D. Application on Real Scene

We have successfully integrated and a surface refinement and projection strategy into our custom-built MM. For our experimental setup, we selected the flat wall as our test area, onto which a water-compatible canvas was placed for painting tasks. The initial operation involved acquiring a surface model of the canvas. Utilizing the proposed 3D surface refinement coupled with a RayCast 3D mapping method, the robot is capable of automatedly generating an end effector painting trajectory for real-time execution.

During the 3D surface model construction phase, the robot calculates the capturing waypoints required for point cloud acquisition. It employs a trajectory controller to navigate directly to these poses. Once the painting trajectory is acquired, the robot seamlessly converts to a whole-body controller. This controller synchronizes the movements of the robot's arm and mobile base to ensure continuous and efficient painting execution.

To accurately assess the real-world performance of the custom MM's ability to follow trajectories, we utilized a motion capture system as the benchmark. The results are displayed in Fig. 12 and Table III. Throughout this process, the robot arm and mobile base constantly compensate for each other's movements to achieve smoother motion. However, it is noted that some tracking precision was compromised due to the mobile base experiencing slight slippage during actual movement. The Root Mean Square Error (RMSE) values for the X, Y, and Z axes were calculated to evaluate the tracking accuracy. Despite the challenges, the robot demonstrated proficient adherence to the preset trajectory, with an overall error margin of 0.046 meters. These results demonstrates both adaptability and precision in real-world robotic painting applications.

VI. Conclusion

Overall, this study represents a mobile manipulator combining with advanced sensing and control technologies to enhance the generation of 3D trajectory surface and adaptive control in indoor applications. The 3D trajectory generation strategy, which combines an Attention-aware Graph Network (AGN) for 3D surface refinement and the RayCast 3D Mapping method, has shown considerable promise in enhancing surface modeling and image mapping accuracy. The adaptive control policy, incorporating both trajectory and closed-loop whole-body controllers, further underscores the mobile manipulator's adeptness in efficiently navigating to target poses and following complex trajectories. However, challenges still persist in real-world environmental dynamics and their impact on the robot's interaction capabilities. Future efforts will focus on real-time environmental adaptability and the motion planning under uncertainty for the mobile manipulator and then expanding its range of operations to encompass more complex tasks.

References

[1] D. Song, J. Park, and Y. J. Kim, "Ssk: Robotic pen-art system for large, nonplanar canvas," *IEEE Transactions on Robotics*, 2023.

[2] J.-P. Sleiman, F. Farshidian, and M. Hutter, "Versatile multicontact planning and control for legged loco-manipulation," *Science Robotics*, vol. 8, no. 81, p. eadg5014, 2023.

[3] A. Iriondo, E. Lazkano, L. Susperregi, J. Urain, A. Fernandez, and J. Molina, "Pick and place operations in logistics using a mobile manipulator controlled with deep reinforcement learning," *Applied Sciences*, vol. 9, no. 2, p. 348, 2019.

[4] E. Asadi, B. Li, and I.-M. Chen, "Pictobot: A cooperative painting robot for interior finishing of industrial developments," *IEEE Robotics Automation Magazine*, vol. 25, no. 2, pp. 82–94, 2018.

[5] D. Song and Y. J. Kim, "Distortion-free robotic surface-drawing using conformal mapping," in *2019 International Conference on Robotics and Automation (ICRA)*. IEEE, 2019, pp. 627–633.

[6] R. K. Megalingam, V. Prithvi Darla, and C. S. Kumar Nimmala, "Autonomous wall painting robot," in *2020 International Conference for Emerging Technology (INCET)*, 2020, pp. 1–6.

[7] B. Zhang, J. Wu, L. Wang, Z. Yu, and P. Fu, "A method to realize accurate dynamic feedforward control of a spray-painting robot for airplane wings," *IEEE/ASME Transactions on Mechatronics*, vol. 23, no. 3, pp. 1182–1192, 2018.

[8] W. Chen, X. Li, H. Ge, L. Wang, and Y. Zhang, "Trajectory planning for spray painting robot based on point cloud slicing technique," *Electronics*, vol. 9, no. 6, p. 908, 2020.

[9] M. Sorour, "Robopainter—a detailed robot design for interior wall painting," in *2015 IEEE International Workshop on Advanced Robotics and its Social Impacts (ARSO)*. IEEE, 2015, pp. 1–6.

[10] W. Lin, A. Anwar, Z. Li, M. Tong, J. Qiu, and H. Gao, "Recognition and pose estimation of auto parts for an autonomous spray painting robot," *IEEE Transactions on Industrial Informatics*, vol. 15, no. 3, pp. 1709–1719, 2019.

[11] M. Ilyas, H. Y. Khaw, N. M. Selvaraj, Y. Jin, X. Zhao, and C. C. Cheah, "Robot-assisted object detection for construction automation: Data and information-driven approach," *IEEE/ASME Transactions on Mechatronics*, vol. 26, no. 6, pp. 2845–2856, 2021.

[12] J. Li, M. Li, Z. Li, and S. Peng, "Super-voxel graph guided 3d point cloud denoising," in *2022 14th International Conference on Computer Research and Development (ICCRD)*. IEEE, 2022, pp. 276–280.

[13] Y. Shen, J. Wang, and I. Puente, "A novel baseline-based method to detect local structural changes in masonry walls using dense terrestrial laser scanning point clouds," *IEEE Sensors Journal*, vol. 20, no. 12, pp. 6504–6515, 2020.

[14] W. Yuan, T. Khot, D. Held, C. Mertz, and M. Hebert, "Pcn: Point completion network," in *2018 International Conference on 3D Vision (3DV)*, 2018, pp. 728–737.

[15] Y. Song, W. Shen, and K. Peng, "A novel partial point cloud registration method based on graph attention network," *The Visual Computer*, vol. 39, no. 3, pp. 1109–1120, 2023.

[16] M. Li, J. Huang, L. Xue, and R. Zhang, "A guidance system for robotic welding based on an improved yolov5 algorithm with a realsense depth camera," *Scientific Reports*, vol. 13, no. 1, p. 21299, 2023.

[17] J. H. M. Lam, K. W. Lo, and Y. Yam, "Robot drawing techniques for contoured surface using an automated sketching platform," in *2007 IEEE International Conference on Automation Science and Engineering*, 2007, pp. 735–740.

[18] S. D. Kundan and G. R. M. Reddy, "Projection and interaction with ad-hoc interfaces on non-planar surfaces," in *2013 2nd International Conference on Advanced Computing, Networking and Security*, 2013, pp. 1–6.

[19] J. Cornejo, J. Palacios, A. Escobar, and Y. Torres, "Mechatronics design and kinematic simulation of utp-isr01 robot with 6-dof anthropomorphic configuration for flexible wall painting," in *2022 First International Conference on Electrical, Electronics, Information and Communication Technologies (ICEEICT)*, 2022, pp. 01–06.

[20] S. Liu, H. Chai, R. Song, Y. Li, Y. Li, Q. Zhang, P. Fu, J. Liu, and Z. Yang, "Contact force/motion hybrid control for a hydraulic legged mobile manipulator via a force-controlled floating base," *IEEE/ASME Transactions on Mechatronics*, 2023.

[21] G. Rizzi, J. J. Chung, A. Gawel, L. Ott, M. Tognon, and R. Siegwart, "Robust sampling-based control of mobile manipulators for interaction with articulated objects," *IEEE Transactions on Robotics*, vol. 39, no. 3, pp. 1929–1946, 2023.

[22] B. Burgess-Limerick, C. Lehnert, J. Leitner, and P. Corke, "An architecture for reactive mobile manipulation on-the-move," in *2023 IEEE International Conference on Robotics and Automation (ICRA)*, 2023, pp. 1623–1629.

[23] S. Thakar, P. Rajendran, A. M. Kabir, and S. K. Gupta, "Manipulator motion planning for part pickup and transport operations from a moving base," *IEEE Transactions on Automation Science and Engineering*, vol. 19, no. 1, pp. 191–206, 2020.

[24] H. Zhang, Q. Sheng, J. Hu, X. Sheng, Z. Xiong, and X. Zhu, "Cooperative transportation with mobile manipulator: A capability map-based framework for physical human–robot collaboration," *IEEE/ASME Transactions on Mechatronics*, vol. 27, no. 6, pp. 4396–4405, 2022.

[25] Q. Sun, S. Li, and X. Kang, "Analysis on kinematics of omnidirectional full drive mobile robot," in *2018 IEEE International Conference on Information and Automation (ICIA)*, 2018, pp. 615–620.

[26] J. Haviland, N. Sünderhauf, and P. Corke, "A holistic approach to reactive mobile manipulation," *IEEE Robotics and Automation Letters*, vol. 7, no. 2, pp. 3122–3129, 2022.